Available online at www.sciencedirect.com
ScienceDirect
Journal of Power Sources 160 (2006) 915–924
JOURNAL OF POWER SOURCES
www.elsevier.com/locate/jpowsour

Characterization and evaluation of Pt-Ru catalyst supported on multi-walled carbon nanotubes by electrochemical impedance

A.L. Ocampo [a], M. Miranda-Hernández [a], J. Morgado [b], J.A. Montoya [b], P.J. Sebastian [a,c,*]

[a] *Centro de Investigación en Energía-UNAM, Temixco, 62580 Morelos, Mexico*
[b] *IMP, Eje Central Lázaro Cárdenas 152, 07730 D.F. Mexico, Mexico*
[c] *Universidad Politécnica de Chiapas, Eduardo J. Selvas, 29082 Tuxtla Gutiérrez, Chiapas, Mexico*

Received 5 January 2006; received in revised form 12 February 2006; accepted 13 February 2006
Available online 5 April 2006

Abstract

In this work the authors present the results of a systematic characterization and evaluation of the carbon nanotube supported Pt-Ru (Pt-Ru/CNT) for its use as methanol oxidation catalyst. Its activity was compared with that of Pt and Pt-Ru catalysts supported on Vulcan and synthesized from carbonyl precursors, and another commercial Pt-Ru catalyst. The cyclic voltammetry, CO stripping and electrochemical impedance techniques were employed to determine the electrocatalytic activity of the catalysts. The electrochemical studies were performed in 0.5 M H_2SO_4 containing different concentrations of methanol (0.05–1 M). The results showed a noticeable influence of the catalyst support (CNT) on the performance of the catalyst for CO oxidation. The electrochemical impedance studies allowed us to separate the different steps in the methanol oxidation reaction and to control these steps or reactions by varying the applied potential and the methanol concentration. At low methanol concentration and potentials the de-hydrogenation of methanol predominated. But, at high potential and methanol concentrations, the CO oxidation predominated. These results allowed us to clearly describe at what potential and concentration ranges the bi-functional effect of Ru becomes evident. Our results indicated that the CO oxidation occurs both on Pt and Ru. Compared to other catalysts, Pt-Ru supported on carbon nanotubes showed superior catalytic activity for CO and methanol oxidation.

Keywords: Carbonyl precursor; CO stripping voltammetry; Electroactive surface area; Pt-Ru electrocatalyst; Direct methanol fuel cell

1. Introduction

In order to satisfy the constant increase in the demand for energy, it is necessary to develop efficient energy production processes and optimize the existing production technologies. Among the new technologies, fuel cells stand out as a potential energy production technology, with the advantage of having a zero or very low emission process. Nevertheless, the commercial application of the fuel cells has been limited by their high cost and in some cases insufficient practical performance. Among the different types, the Direct Methanol Fuel Cell (DMFC) is very promising for portable applications and in electrical vehicles.

Methanol is a liquid fuel which provides high energy density and has important advantages over hydrogen in terms of storage, transportation, and cost [1,2]. However, the main factors that limit and diminish the practical performance of the DMFC are the slow kinetics of methanol oxidation and the poisoning of the anode catalyst. In order to surpass these problems, catalysts with higher catalytic activity are necessary. Pt is a good catalyst for methanol oxidation; however, it is quickly poisoned by the CO reaction intermediates [3–6]. Superior catalytic activities have been reported for Pt based alloys, such as Pt-Ru, Pt-Mo, Pt-Sn, Pt-Os, Pt-Ru-Os, etc. [4,7–10]. This enhancement effect has been explained by models such as the "bifunctional mechanism" [11–14] and/or by the "electronic effect" [15–17], which indicates a promotional effect of the alloyed metal on Pt. Particularly, Pt-Ru has been the most investigated binary system, and has shown the best catalytic activity [8,14,18–20]. Nevertheless, the search for the optimum catalytic activity for Pt-Ru catalyst

* Corresponding author. Tel.: +52 777 3250052x29706; fax: +52 777 3250018.
E-mail address: sjp@cie.unam.mx (P.J. Sebastian).

0378-7753/$ – see front matter © 2006 Elsevier B.V. All rights reserved.
doi:10.1016/j.jpowsour.2006.02.056

continues being a subject of active research. There are several factors that influence the physical properties and the electrochemical performance of the Pt-Ru catalyst [8,14,21]: (1) the preparation method, (2) the atomic ratio between platinum and ruthenium, (3) the nature of the catalyst support, and (4) an optional heat treatment, are the important ones. Other important factors such as the particle size, the morphology, the electrochemically active area, and the crystalline phase influence the physical properties.

The chemical or electrochemical reduction of the metallic ions from their salts has been the most common method for the synthesis of Pt-Ru in its supported or unsupported form. A new preparation method of the binary catalyst was reported by Dickinson et al. [22] who used carbonyl compounds as metal precursors. From the synthesis of a complex platinum carbonyl and combining it with a ruthenium carbonyl compound and carbon (Vulcan XC-72R) in a thermolysis reaction, they produced a carbon supported catalyst. The authors of the research presented here followed this methodology, with the difference that we used multi-walled carbon nanotubes as support material, and in addition, we submitted the catalysts to a heat treatment in a hydrogen atmosphere to improve their catalytic properties.

Recently the importance of catalyst support for fuel cells has been recognized and different forms of carbon have been suggested [23–25]. The structure, surface area, and porosity are factors that directly affect the performance of the catalysts [23–25]. The application of carbon nanotubes as support for the fuel cell catalysts has been a subject of great interest during the last few years [24–27]. Their high surface area is a very important characteristic because of a better dispersion of the catalyst, which generally entails a better catalytic activity. Pt-Ru nanoparticles have been either electrodeposited on carbon nanotube or impregnated on multi-walled and single-walled carbon nanotubes, obtaining high electrocatalytic activity for methanol oxidation [24,26].

In order to determine the catalytic activity of the anode catalysts, and to characterize the processes taking place at the anode and cathode of a DMFC, the electrochemical impedance spectroscopy (EIS) has been used recently as a powerful tool by some researchers under real operating conditions. Using simple equivalent circuits, the impedance behavior corresponding to the anode and cathode processes have been explained [28–30] showing this technique as a useful tool for the development of the DMFCs. Methanol oxidation has been investigated by EIS technique using a variety of catalysts: polycrystalline platinum [31,32], carbon supported Pt [33,34], Pt-Ru [35], and Pt-Sn [36] in acid media, and a cobalt hydroxide modified glassy carbon electrode in alkaline media [37]. However, there has been no report on the impedance characteristics of carbon nanotube supported Pt-Ru catalyst. In the present study, we applied the EIS technique for the electrochemical characterization of methanol oxidation on Pt-Ru catalysts supported on a multi-walled carbon nanotube (Pt-Ru/CNT). CO stripping experiments were also used to characterize its performance of CO oxidation and to determine its electroactive surface area.

2. Experimental details

2.1. Catalyst preparation

The synthesis of the catalyst was performed following the method described by Dickinson et al. [22]. The precursors used were Pt carbonyl complex ($[Pt_3(CO)_6]_n^{2-}$) and commercially available Ru carbonyl, [$Ru_3(CO)_{12}$, Aldrich]. To prepare a Pt carbonyl complex, there are a number of reports in the literature [22,38,39]. Pt carbonyl complex was firstly prepared by purging CO through an aqueous solution of chloroplatinic acid (H_2PtCl_6, Aldrich) for 24 h with constant mechanical stirring. After that, the Pt carbonyl precursor was mixed with Ru carbonyl and commercial multi-walled carbon nanotubes (MER Corporation, Arc-produced MWNT). Nanotubes were 6–20 nm in diameter and 1–5 μm in length, and they were used as received. Then the mixture was refluxed in *o*-xylene in a round bottom flask at 143 °C for 24 h with constant mechanical stirring. At the conclusion of the reaction, the mixture was allowed to cool down to room temperature. Later on, the *o*-xylene was removed by a vacuum method and the catalyst was let to dry for several days. The precursor quantities were chosen to obtain a 50:50 Pt:Ru atomic ratio. An additional step to the Dickinson's method was to submit the catalyst to a thermal treatment in a hydrogen atmosphere at 300 °C for 3 h. For the sake of comparison the Pt-Ru (50:50) and Pt catalysts supported on Vulcan (XC-72C Cabot) were prepared following the methodology described earlier. In all the cases the catalysts amount in carbon was 20 wt.%.

To prepare the electrode, 1 mg of the catalyst was mixed with 10 μl of Nafion solution (in 5% of aliphatic alcohols, Electrochem Inc.) and diluted in isopropanol in an ultrasonic bath. From the resulting ink, 5 μl was deposited as a thin film on a graphite rotating disk electrode (rde) with a cross-sectional area of 0.19 cm^2.

2.2. Physical characterizations

In a Siemens diffractometer with Cu Kα radiation (1.5406 Å wave length) operated at 35 keV and 25 mA, X-ray diffraction (XRD) patterns were obtained at a rate of 2° min^{-1} for values of 2θ between 10° and 90°. The peak Pt(2 2 0) was used to determine the average particle size using the Scherrer equation [40].

The Transmission Electronic Microscopy (TEM) images were obtained through a JEOL JEM – 2010F Microscope operated at 200 keV. The Pt-Ru/CNT catalyst was deposited on a copper grid. High resolution images were also obtained (HRTEM).

2.3. Electrochemical measurements

For the electrochemical experiments a glass cell with a three electrode configuration was used. A Saturated Mercury Sulphate Electrode (SSE) placed within a capillary luggin was used as the reference electrode. The counter electrode used was a graphite bar and the working electrode was the rde containing the catalyst. All potentials reported in this work were corrected with respect to the Normal Hydrogen Electrode (NHE). Half cell data were

obtained using a Solartron Electrochemical Interface (model IF 1287) and the Correware software.

In order to determine the catalytic activity of the Pt-Ru/CNT for methanol oxidation, cyclic voltammetry (CV), EIS, and CO stripping experiments were carried out at room temperature (23 ± 1 °C). For the CO stripping voltammetry, carbon monoxide (chemically pure) was absorbed onto the Pt-Ru/CNT catalyst by bubbling it into the supporting electrolyte (0.5 M H_2SO_4) for 20 min, while the potential was held at 0.15 V/NHE. To remove the CO dissolved in the electrolyte a N_2 purge was applied with the potential still held at 0.15 V. The experimental conditions of CO absorption time and potential were taken from the literature [41] and considering that at this potential there is no spontaneous CO adsorption or oxidation. The potential was then cycled starting at 0.15 V for three cycles at 10 mV s^{-1}.

EIS experiments were carried out in 0.5 M H_2SO_4 with different methanol concentrations (1.0, 0.5, 0.1 and 0.05 M). The impedance spectra were registered at frequencies from 10^3 to 10^{-3} Hz with a logarithmic data collection at seven steps per decade with amplitude of 10 mV at the desired potential. During measurements, the rde was rotating at 1600 rpm to establish a constant diffusion regime. For impedance measurements an impedance analyzer IF 1260 and the Z-plot and Z-view softwares were used.

3. Results and discussion

3.1. XRD and TEM characterization

Fig. 1 show the XRD patterns for the catalysts, Pt-Ru/CNT (Pt-Ru supported on carbon nanotube), Pt-Ru/C (Pt-Ru supported on Vulcan), Pt/C (Pt supported on Vulcan) and the commercial catalyst PtRu/C_{com} (Electrochem, 20 wt.% Pt, 10 wt.% Ru, supported on Vulcan). All the catalysts, except the commercial Pt-Ru, were synthesized via the same route (starting from the carbonyl precursors of Pt and Ru). The XRD patterns of the catalysts were compared with the standard patterns of Pt (JCPDS, card 4-802) and Ru (JCPDS, card 6-663). The diffraction peaks in all the diffractograms indicate the presence of the face centered cubic (fcc) structure of Pt represented by the planes (1 1 1), (2 0 0), (2 2 0), (3 1 1), and (2 2 2) (JCPDS, card 4-802). In the case of Pt-Ru/CNT, the diffraction peaks around 26°, 42° and 54° are attributed to the hexagonal structure of graphite (0 0 2), (1 0 0), and (0 0 4) [25,27]. In addition, only in the case of Pt-Ru/CNT diffraction peaks were observed at 44° (1 0 1) and 78° (1 0 3), those were assigned to hcp structure of Ru (JCPDS, card 6-663), which is shown as the dotted line in the figure. These results indicate that Pt and Ru are in separate phases. Nevertheless, the diffraction peaks Pt(1 1 1) and Pt(2 2 0) for Pt/C are observed at 2θ values, 39.8° and 67.5°, respectively, where as for the Pt-Ru catalyst these peaks are seen displaced to higher angles, particularly for Pt-Ru/CNT they are at 40.2° and 68.2°. This displacement of the peaks indicates the formation of Pt-Ru in an alloyed phase [41]. The lattice parameter (a_{fcc}) is useful to show the formation of the Pt-Ru alloyed phase in the fcc structure. The reported values of a_{fcc} for Pt/C are between 3.9155 and 3.9244 Å [6,42,43], where as in the present study the value of a_{fcc} is 3.921. Meanwhile for the Pt-Ru alloy there exists a decrease in a_{fcc} values due to the smaller size of Ru incorporated in the fcc structure of Pt [6]. For PtRu/C_{com}, Pt-Ru/C and Pt-Ru/CNT, the values of a_{fcc} are 3.8931, 3.8936 and 3.886 Å, respectively, which indicates the formation of the Pt-Ru alloy. However, with Pt-Ru/CNT also there exist the separate phases of Pt and Ru, as seen in the diffractogram.

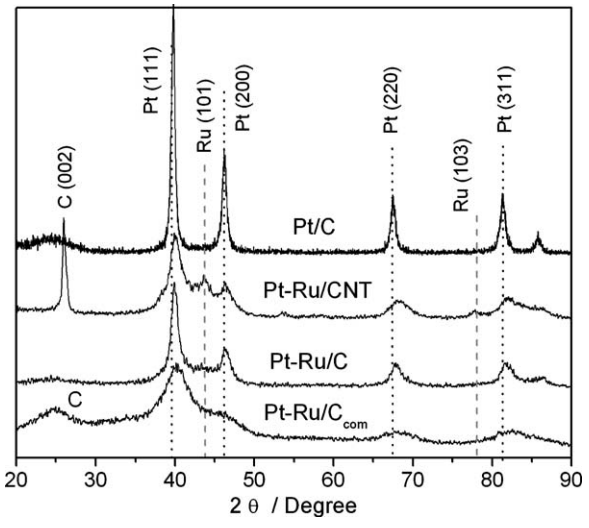

Fig. 1. Patterns of X-ray diffraction of the Pt/C and Pt-Ru/CNT catalyst.

In Fig. 2, TEM images are shown of the morphology of the PtRu/CNT catalyst. In Fig. 2a, small particles of Pt-Ru stuck to the carbon nanotube are observed. However, its distribution is not very homogeneous. In Fig. 2b, a high resolution TEM image is presented. The form and size of the particles are not well defined, possibly due to a certain agglomeration of the particles or to the strong interaction of the support material with the particles under the conditions of the sampling equipment. The particle size was estimated at approximately 5 nm, greater than the value determined by XRD due to the scant definition of the particles. Crystalline graphite planes are clearly observed. Also, the Pt-Ru particles deposited show lattice fringes for which further information was not obtained regarding the parameters of lattice, ordering and orientation in order to determine whether the particles correspond to the Pt, to the Ru or to a bi-metallic Pt-Ru particle.

3.2. CO stripping voltammetry study

Fig. 3a corresponds to the cyclic voltammetry during the first 3 cycles after the catalyst (Pt-Ru/CNT) was pre-absorbed with CO for 20 min at 0.15 V. The scanning potential was initiated in the anodic direction. As the scanning progressed, one could observe an anodic peak corresponding to the oxidation of CO_{ads}. In the following cycles this peak is no longer present, which indicates that all of the CO absorbed was completely unabsorbed during the first cycle. The onset potential and peak potential for the oxidation of CO_{ads} are 0.34 and 0.46 V, respectively. For the sake of comparison, Fig. 3b presents the CO stripping voltammograms on Pt-Ru/C_{com}, Pt-Ru/C, Pt/C along with the

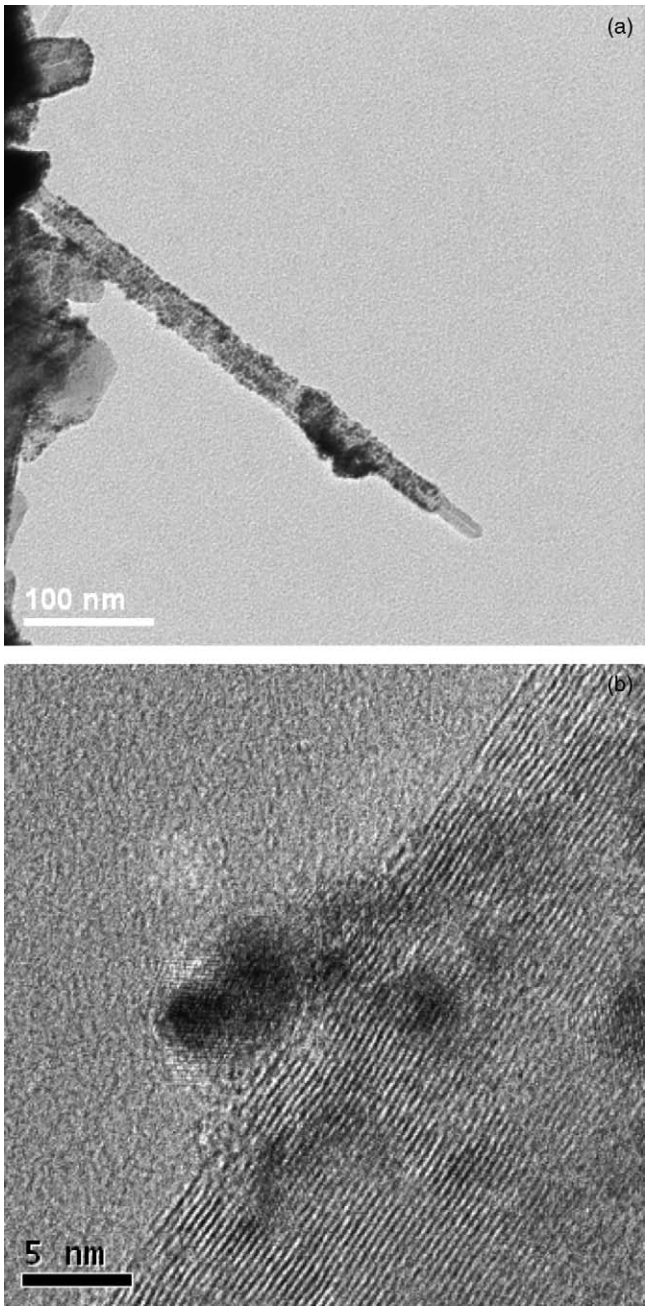

Fig. 2. TEM images of the Pt-Ru/CNT (a) low resolution and (b) high resolution.

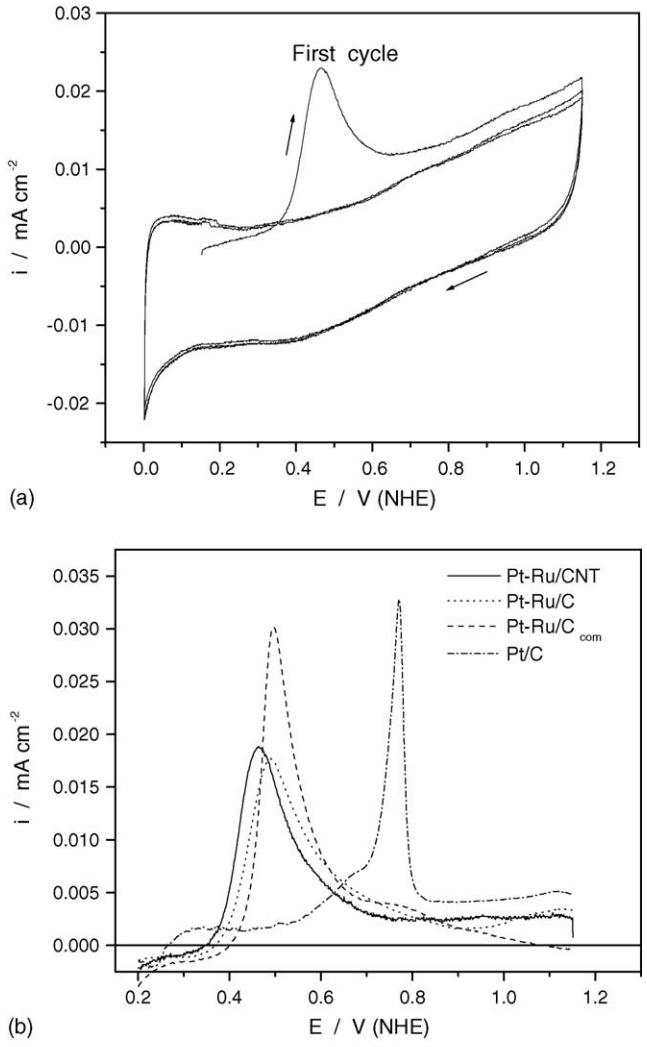

Fig. 3. (a and b) CO_{ads} stripping voltammograms recorded at 10 mV s^{-1} in 0.5 M H_2SO_4.

voltammogram for Pt-Ru/CNT. One can observe in Fig. 3b that the characteristic of the oxidation peak of CO_{ads} depends on the nature of the catalyst. The onset potential for the oxidation of CO_{ads} is similar for PtRu/C_{com}, PtRu/C and PtRu/CNT, but for Pt/C this potential is more positive, which implies a higher overpotential. The oxidation peak for CO_{ads} is observed at 0.5 V for all the catalysts that contain Ru except Pt-Ru/CNT. For Pt-Ru/CNT the oxidation peak of CO_{ads} is more negative, which indicates that the CO_{ads} oxidation becomes energetically more favorable. In other words, one can say that Pt-Ru/CNT is catalytically more efficient than the other catalysts. In the meantime the peak potential for CO_{ads} oxidation on Pt/C remains at 0.77 V as reported by other authors [44–47].

After the oxidation peak, the current falls and stays at a constant value. The current value depends on the type of the catalyst, which means there are still absorbed species on the catalyst surface, with Pt/C having more current than Pt-Ru/C and Pt-Ru/CNT. Similar characteristics for these catalysts have been reported by other authors also [48]. The peak shape is similar for all the catalysts, a broad peak indicates a slow oxidation reaction. In the case of Pt/C, the peak shape is symmetric and sharp, which indicates a fast oxidation reaction, but the reaction takes place at potentials which are not adequate for the proper functioning of a direct methanol fuel cell.

The displacement of the onset and peak potentials in a negative direction in the case of the catalysts containing Ru compared to Pt/C is mainly related to the bi-functional mechanism [49], where the beneficial effect is related to the formation of Ru-OH species at low potentials, which facilitates the complete oxidation of adsorbed CO as was reported by others [9,50,51]

$$Ru + H_2O \rightarrow (OH)_{ads} + H^+ + e^- \quad (1)$$

$$(CO)_{ads} + (OH)_{ads} \rightarrow CO_2 + H^+ + e^- \quad (2)$$

This confirms the important role of Ru in the oxidation of CO and hence that of methanol. Also, the above results indicate the importance of the support material for a better performance of the catalyst, especially in the case of carbon nanotubes.

3.3. Evaluation of the electroactive area

From Fig. 3b the area under the curve was determined. This area corresponds to the amount of charge related to the oxidation of CO adsorbed on the catalyst surface. The voltammetric area (without CO adsorption) was subtracted from the CO stripping area to eliminate the contributions of the double layer region. To determine the electroactive area the value of 420 $\mu C\,cm^{-2}$ was used as the oxidation charge of one monolayer of adsorbed CO on a smooth Pt surface [52–54]. Table 1 gives the summary of the parameters such as onset potential, peak potential, the charge associated with oxidation of CO_{ads} and the electroactive area, extracted from the CO stripping curves. From Table 1, one can observe that Pt-Ru/CNT has the best characteristics for the onset and peak potential. But, this catalyst shows low charge associated with the CO_{ads} oxidation and hence a lower electroactive area compared to the catalysts, Pt-Ru/C and Pt-Ru/C_{com}. The Cu stripping has been reported as an adequate technique to determine the electroactive area of Pt-Ru catalysts due to the similarities in the atomic radii of these elements (Cu-0.128 nm, Pt-0.135 nm, Ru-0.134 nm) and assuming that each atom of Cu adsorbed is equivalent to a superficial metallic atom of Pt or Ru [55]. It is also generally accepted that the CO adsorption on Pt is effected through a linear bond 1:1, in the case of Ru it is reported that this interaction can be via a linear bonding or the bridge bonding, where the CO:Ru bonding relation can be up to 2:1 [52]. Hence the adsorption of CO on Pt-Ru may not be considered as the 1:1 type. Considering the fact that in the present study, the bi-metallic catalyst and the catalyst support are nanostructured materials and taking into account arguments presented with respect to the atomic radii and bond type, it is possible that the considerations made in the determination of the electroactive area may not be correct for these kinds of catalysts and that we need to look for another methodology to evaluate their electroactive area.

3.4. Electrochemical impedance characterization of Pt-Ru/CNT

The electrochemical impedance characterization of the oxidation of methanol on Pt-Ru/CNT catalyst was done in 0.5 M H_2SO_4 with different concentrations of methanol and by applying different potentials. These studies were done in a frequency range of 10^3 to 10^{-3} Hz, with amplitude of 10 mV and from stationary state to 1600 rpm.

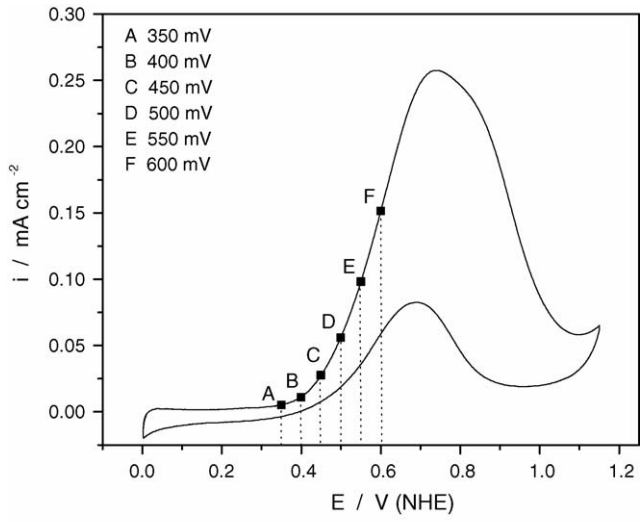

Fig. 4. Cyclic voltammograms for Pt-Ru/CNT in 1 M CH_3OH/0.5 M H_2SO_4 showing the selected potentials for EIS experiments.

3.4.1. Effect of applied potential

Fig. 4 shows the voltammetric response corresponding to a potential sweep of 10 $mV\,s^{-1}$ and 1600 rpm in 1 M CH_3OH/0.5 M H_2SO_4 for the Pt-Ru/CNT deposited on a rotating disc electrode. From this response the potentials at which the impedance studies would be done were selected, which are indicated in Fig. 4. The potential interval selected was 350–600 mV with an increment of 50 mV. Fig. 5 gives the impedance spectra for the above-mentioned system. The complex plane plot of the impedance spectra is shown in Fig. 5a and the Bode plot is given in Fig. 5b. In the complex plane impedance plot, a semicircle which cuts the real axis is observed. The diameter of this semicircle decreased as the applied potential increased and an inductive loop appeared at low frequencies (see the insert figure). Similar results have been reported for Pt and Pt-Ru [33–35], where the inductive effect was attributed to the kinetics of the electrooxidation of methanol, in particular, to the CO oxidation. On the other hand, the Bode diagram showed that the phase angle is independent of the applied potential in the frequency range 1000–10 Hz. At low frequency ranges, the phase angle shows a maximum; its value depends on the applied potential as well as frequency. The maximum phase angle is obtained when the applied potential is the lowest. As the electrode potential is increased, the maximum

Table 1
CO_{ads} stripping characteristics and electroactive areas determined from the charge to oxidize a monolayer of CO on Pt and Pt-Ru catalysts

Catalyst	E_{onset} (V)	E_{peak} (V)	Charge (C)	Electroactive area[a] (cm^2)	Electroactive area ($m^2\,g_{Pt}^{-1}$)
Pt/C	0.5	0.77	1.04×10^{-3}	2.5	6
Pt-Ru/C_{com}	0.4	0.5	1.02×10^{-2}	24	30
Pt-Ru/C	0.37	0.49	9.5×10^{-3}	23	29
Pt-Ru/CNT	0.34	0.46	1.7×10^{-3}	4	5

[a] Equivalent to a geometric area of 0.19 cm^{-2}.

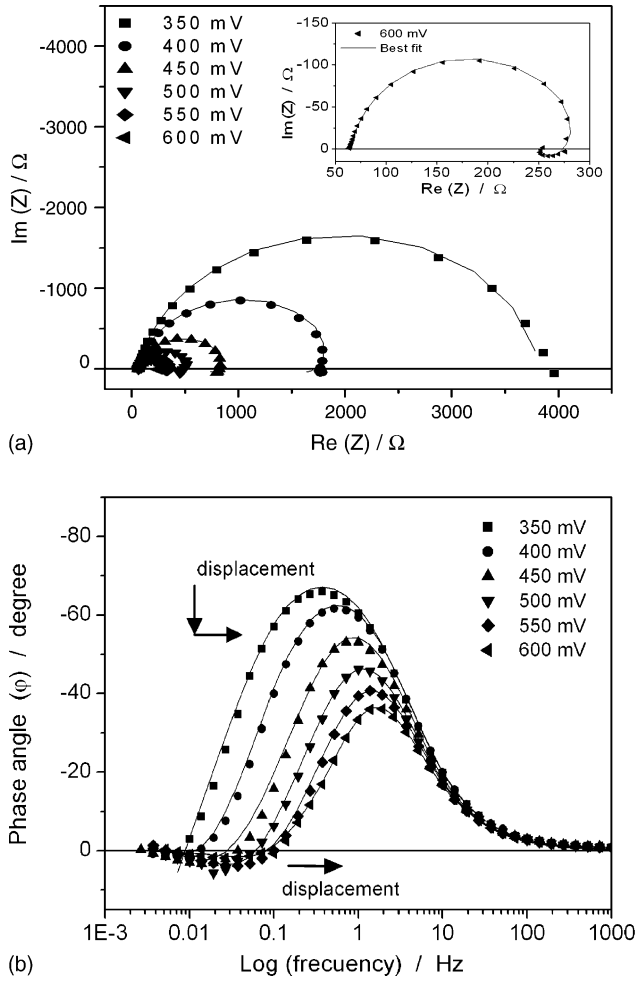

Fig. 5. (a) Complex plane impedance plots in 1 M CH_3OH/0.5 M H_2SO_4 at various electrode potentials, (b) the corresponding Bode plots. Solid lines represent the fitted data to the equivalent circuit of Fig. 6.

in phase angle decreased and shifted to higher frequencies (see the direction of the arrow in Fig. 5b). It is also seen in Fig. 5b that the amplitude of the phase angle extends more than one frequency decade, which is attributed to the multiple processes interrelated by their time constants. Similar responses have been reported for coupled reactions [56]. In the case of responses obtained for frequencies below 0.1 Hz, the phase angle values cross the frequency axis and move towards positive values. Also, in this case we observed a maximum in positive values of phase angle and a displacement towards higher frequencies for the phase angle where it crosses the frequency axis. Similar characteristics for the variation of phase angle with frequency have been reported earlier by Hsing et al. [34] and Sugimoto et al. [35], where the two maxima (for positive and negative phase angle values) represent the existence of two different time constants [34]. The time constant at high frequencies corresponds to the occurrence of a fast reaction step and that of low frequencies corresponds to a slow reaction step. The methanol oxidation reaction on Pt-Ru may be described as [4,57]

$$Pt + CH_3OH \rightarrow Pt\text{–}(CH_3OH)_{ads} \quad (3a)$$

$$Pt\text{–}(CH_3OH)_{ads} \rightarrow Pt\text{–}(CH_3O)_{ads} + H^+ + e^- \quad (3b)$$

$$Pt\text{–}(CH_3O)_{ads} \rightarrow Pt\text{–}(CH_2O)_{ads} + H^+ + e^- \quad (3c)$$

$$Pt\text{–}(CH_2O)_{ads} \rightarrow Pt\text{–}(CHO)_{ads} + H^+ + e^- \quad (3d)$$

$$Pt\text{–}(CHO)_{ads} \rightarrow Pt\text{–}(CO)_{ads} + H^+ + e^- \quad (3e)$$

$$Ru + H_2O \rightarrow Ru\text{–}(H_2O)_{ads} \quad (4)$$

$$Ru\text{–}(H_2O) \rightarrow Ru\text{–}(OH)_{ads} + H^+ + e^- \quad (5)$$

$$Pt\text{–}(CO)_{ads} + Ru\text{–}(OH)_{ads} \rightarrow Pt + Ru + CO_2 + H^+ + e^- \quad (6)$$

Considering these reactions, the time constants at high frequencies can be related to the de-hydrogenation of methanol (Eqs. (3a)–(3e) and those at low frequencies may be related to the CO_{ads} oxidation velocity (Eq. (6)). On the other hand, Sugimoto et al. [35] attributed these maxima in phase angle values to the transitions occurring from the capacitive to resistive characteristics (high frequencies) and resistive to inductive characteristics (low frequencies). These displacements in phase angles signify the fact that the reaction velocities for de-hydrogenation of methanol and CO oxidation are increased with an increase in applied potential.

The impedance results were converted into equivalent electrical circuits using the Equivalent Circuit program available with the potentiostat (EG&G-PARC, Version 4.51). The fitted impedance curves correspond to the solid lines in Fig. 5. Two equivalent circuits were generated for this effect. The first one (Fig. 6a) corresponds to the potential interval 350–450 mV and the second one (Fig. 6b) to the potential interval 500–600 mV. In Fig. 6, R_s represents the solution resistance, CPE1 the constant phase element associated with the double layer capacitance, R_{ct} the charge transfer resistance associated with methanol oxidation, R_o and L are associated with the adsorption processes of intermediates formed during methanol oxidation and CPE2 and R_∞ are associated with the CO_{ads} oxidation.

Table 2 gives the values of the components of the electrical equivalent circuits corresponding to the impedance results (Fig. 5) obtained for Pt-Ru/CNT in 1 M CH_3OH/0.5 M H_2SO_4. It is seen in Table 2 that the electrolyte resistance (R_s) is con-

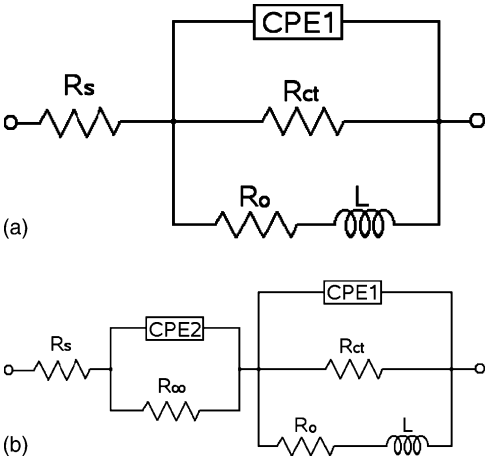

Fig. 6. Equivalent circuit for modeling electrochemical impedance of Pt-Ru/CNT in 1 M CH_3OH/0.5 M H_2SO_4 for potentials (a) from 350 to 450 mV and (b) from 500 to 600 mV.

Table 2
Electrical element values of the equivalent circuit of the impedance plot for Pt-Ru/CNT in 1 M CH_3OH/0.5 M H_2SO_4 at various electrode potentials

Potential (mV)	R_s (Ω)	R_{ct} (Ω)	$C1$ (F)	$C2$ (F)	R_∞ (Ω)	R_o (Ω)	L (H)
350	65	3.9×10^3	8.54×10^{-4}	–	–	–	–
400	66	2×10^3	7.9×10^{-4}	–	–	6×10^3	6.5×10^4
450	67	8.5×10^2	8×10^{-4}	–	–	2.8×10^3	2×10^4
500	68	5×10^2	8.2×10^{-4}	4.3×10^{-2}	1.3×10^2	1.2×10^3	4.4×10^4
550	61	3.2×10^2	8.5×10^{-4}	1.08×10^{-2}	8.9×10^1	9.6×10^2	2.2×10^3
600	64	2.1×10^2	9.5×10^{-4}	4×10^{-3}	2×10^1	8.3×10^2	2×10^3

stant for the whole interval of applied potential, which indicates that the electrolyte conductivity does not change. The R_{ct} value associated with the de-hydrogenation of methanol (steps a–e of reaction (3)) diminished with increasing potential. Considering the voltammetric response shown in Fig. 4, it is observed that as the potential increased (during the applied potential interval of interest) towards more positive values the methanol dehydrogenation reaction seems less important and gradually the CO oxidation reaction predominates. This is due to the progress of the reactions coupled with the CO oxidation on Pt in such a way that these effects are reflected in the variation of R_{ct}, i.e., R_{ct} diminishes as the applied potential increases.

In the case of the constant phase elements, the value of n was >0.9 in all cases. With this, the real values of capacitance were evaluated and are shown in Table 2. The double layer capacitance values $C1$ are almost constant during the whole interval of applied potential, but, it is important to mention that their values are higher than those reported normally for the double layer capacitance (10^{-6}–10^{-5} F). This may be explained by the fact that this parameter ($C1$) involves other contributions such as the adsorption of the carboxylated species, the product of the dehydrogenation of methanol (reaction (3a)–(3e), which promotes and takes place during the applied potential range. This result is in accordance with the voltammetric response of Fig. 4. R_o and L are associated with the limiting step of reaction (6), the oxidation of CO on Pt. The decrease in their values with increasing potential is attributed to the fact that the velocity of CO oxidation is more rapid with increasing applied potential. Finally, $C2$ and R_∞ (Fig. 6b) are defined only when the impedance response corresponds to higher potentials. These elements of the equivalent circuit describe the adjustment of the total inductive response at very low frequencies and it is considered that they describe the oxidation process of CO on sites different from Pt, i.e., CO oxidation on Ru sites.

3.4.2. *Effect of methanol concentration*

The EIS studies were carried out in 0.5 M H_2SO_4 at different concentrations of methanol (0.05, 0.1, 0.5 and 1 M). The impedance response was obtained for each concentration of methanol and for different applied potentials. Fig. 7 displays a comparison of the responses obtained for different concentrations of methanol at 500 mV. The complex plane plot of the data (Fig. 7a) shows a semicircle for all the concentrations. For the higher concentrations (0.5 and 1 M) the diameter of the semicircle decreased and at low frequencies an inductive loop is observed (see insert figure).

The Bode plot (Fig. 7b) shows that at high frequencies, the phase angle is independent of the concentration (except for the 0.1 M, possibly due to a change in the mechanism or an additional step for this concentration). As low frequencies are reached, a maximum in the phase angle is obtained, which depends on the methanol concentration and frequency. The impedance response may be divided into two parts; the ones at high methanol concentrations and the others at low concentrations of methanol. For the higher concentrations of methanol, the maxima in phase angle shows lower values compared to that of lower concentrations and are displaced towards higher frequencies. At low frequencies, the higher concentrations show positive phase angle values, which corresponds to the inductive effect shown in Fig. 7a. It is important to mention that for the

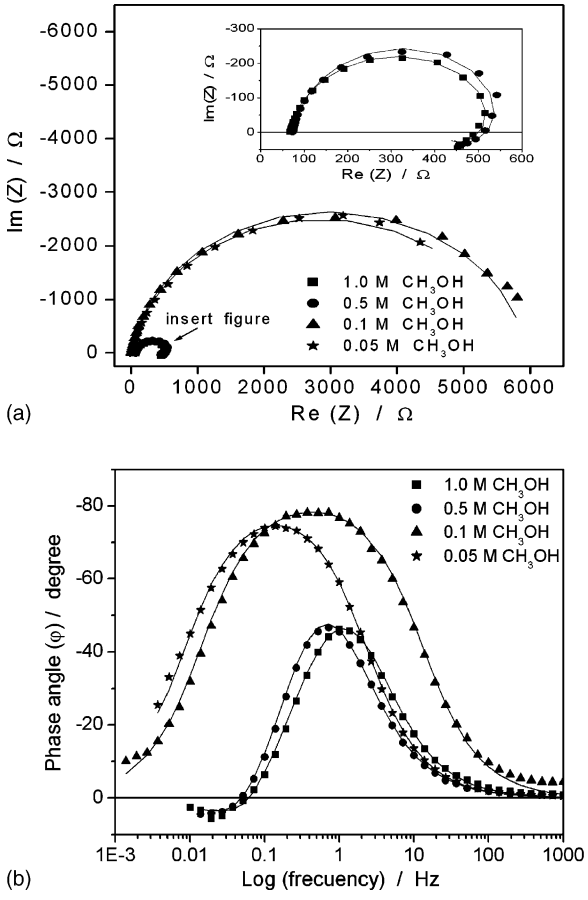

Fig. 7. (a) Complex plane impedance plots in 0.5 M H_2SO_4 for different methanol concentrations and at 0.5 V electrode potential and (b) the corresponding Bode plots. Solid lines represent the fitted data to the equivalent circuit.

Table 3
Electrical element values of the equivalent circuit of impedance plot for Pt-Ru/CNT in 0.5 M H_2SO_4 for different methanol concentrations at 500 mV

Methanol conc. (M)	R_s (Ω)	R_{ct} (Ω)	$C1$ (F)	$C2$ (F)	R_∞ (Ω)	R_o (Ω)	L (H)
1.0	68	5×10^2	8.2×10^{-4}	4.3×10^{-2}	1.3×10^2	1.2×10^3	4.4×10^4
0.5	73	4.7×10^2	1.4×10^{-3}	2.7×10^{-3}	3.3×10^1	1×10^3	5×10^3
0.1	11	6×10^3	1.5×10^{-3}	–	–	–	–
0.05	32	5.6×10^3	2.6×10^{-3}	–	–	–	–

lower concentrations, no inductive effect was observed for any applied potential. Along these lines, Jafarian et al. [37] have reported similar results for methanol concentrations between 0.05 and 0.5 M, while the inductive effect appeared for higher concentrations.

The equivalent circuits used to simulate the impedance response at higher concentrations of methanol are shown in Fig. 6. For the lower concentrations, a new equivalent circuit, shown in Fig. 8, was used for the whole applied potential interval. Since there appeared to be no inductive effect for the lower concentrations, the equivalent circuit contains only R_s, CPE1 and R_{ct}, with the previously mentioned characteristics.

Table 3 gives the values of the equivalent circuit elements obtained for different concentrations of methanol for an applied potential of 500 mV. In all the cases, R_s changes, which is logical since the electrolyte concentration is different in each case, and hence the electrolyte conductivity. Comparing Tables 2 and 3, it can be observed that, for low methanol concentrations and low applied potentials, the R_{ct} values are similar, which means the de-hydrogenation of methanol is predominant. For higher applied potentials (450–600 mV) and high methanol concentrations, the reaction velocity for methanol de-hydrogenation and CO oxidation increase. This indicates that the global reaction speed for methanol oxidation can be promoted by the applied potential as well as the methanol concentration.

The $C1$ values tend to increase with the decrease in methanol concentration, which indicates a higher influence by the species produced during the de-hydrogenation of methanol at low concentrations. In this case, the $C1$ values are higher than those normally reported for the double layer, which indicates that there is an effect due to the concentration of the species adsorbed on the electrode surface, as was observed in the case of the effect due to the applied potential (Table 2). R_o and L were defined for the higher concentrations, but their values indicate a higher CO oxidation speed for the methanol concentration of 0.5 M. The elements $C2$ and R_∞ were present only for high concentrations and it is noteworthy that their order of magnitude is similar in the case of higher potentials (Table 2), which indicates that these elements correspond to the same process promoted by higher potentials and concentrations of methanol. As was discussed in the previous section, it is possible that in these conditions there can be a higher participation of Ru as catalyst and that the CO oxidation takes place on Ru also, which induces the appearance of a new process reflected in $C2$ and R_∞.

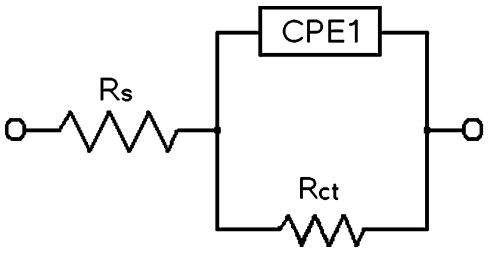

Fig. 8. Equivalent circuit for modeling electrochemical impedance of Pt-Ru/CNT in 0.5 and 1 M CH_3OH/0.5 M H_2SO_4 for the whole interval of applied potential.

To compare the kinetics of methanol oxidation, a summary of the charge transfer resistance per unit area as a function of applied potential and methanol concentrations is presented in Table 4. For all the concentrations, the R_{ct} values diminish as the potential increase, which, as discussed earlier, is attributed to the increase in the speed of methanol de-hydrogenation and CO oxidation. It is also observed that at low concentrations, the resistance values are very high, especially at low potentials where the de-hydrogenation of methanol dominates. At low concentrations and high potentials, the favored reaction is CO oxidation. Similar tendencies have been reported in the response of the charge transfer resistance in the case of PtRu/C in 1 M CH_3OH/0.5 M H_2SO_4 at 60 °C, for the potentials from 300 to 550 mV [35]. For Pt/C (50 wt.%), Otomo et al. [33] have reported a decrease in R_{ct} value during the interval 350–600 mV, and observed that at higher potentials, R_{ct} increased again. They also reported that, for methanol concentration in the range of 0.05–1.0 M, the R_{ct} values diminished drastically while for the concentration range 2.0–10.0 M, the decrease in R_{ct} was slower. For Pt-Ru supported on carbon nanotubes, there were no reported data for R_{ct} values.

Through the impedance analysis it has been possible to describe the mechanism of methanol oxidation in 0.5 M H_2SO_4, controlling the different parameters. The results demonstrated the bi-functional effect of Pt-Ru/CNT catalyst in the methanol oxidation. Hence Pt-Ru/CNT may be considered as an alternative catalyst/support system for the anode of the direct methanol fuel cell.

3.5. Cyclic voltammetry of methanol oxidation

Fig. 9 displays a comparison of catalytic activity for Pt-Ru/C_{com}, Pt-Ru/C, and Pt-Ru/CNT catalysts in 1 M CH_3OH/0.5 M H_2SO_4. The onset potential for methanol oxidation is very similar for all the catalysts (350–400 mV), which corresponds well with the results shown in Fig. 3b for the onset potential for CO oxidation, and also with the inductive effect shown in the impedance results. The peak potential is slightly smaller for Pt-Ru/C and Pt-Ru/CNT. The catalytic activity is similar for the catalysts, Pt-Ru/CNT and Pt-Ru/C_{com} with

Table 4
Charge transfer resistance for methanol oxidation obtained from Impedance measurements

Potential (mV)	Charge transfer resistance R_{ct} (Ω cm^{-2})			
	1.0 (M)	0.5 (M)	0.1 (M)	0.05 (M)
350	970.2	855.7	4328.4	3124.4
400	532.3	462.7	2395.5	2231.3
450	211.4	248.8	2059.7	1741.3
500	126.7	117.7	1477.6	1403
550	78.4	78.6	–	–
600	52.7	54.5	–	–

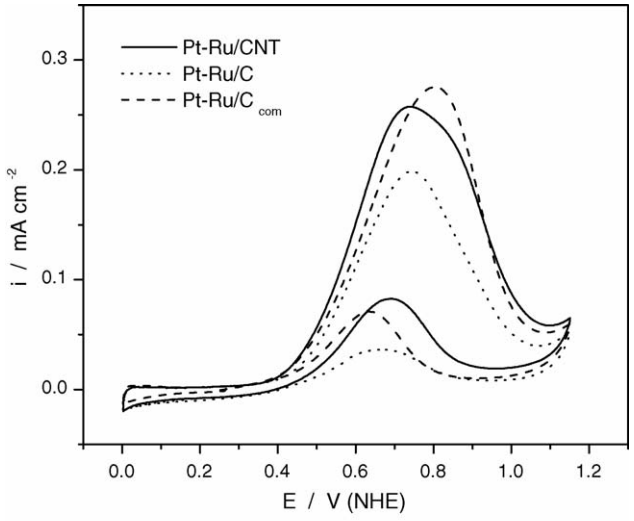

Fig. 9. Cyclic voltammograms for the different Pt-Ru catalysts; straight line for the carbon nanotube supported, dash line for the commercial, and dotted line for the carbon (Vulcan) supported, in 1 M CH_3OH/0.5 M H_2SO_4 with a scan rate of 10 mV s^{-1}.

values 0.26 and 0.27 mA cm^{-2}, respectively, at the peak potential. Similar to the results obtained for CO oxidation, a better electrocatalytic response was obtained for methanol oxidation on catalysts supported on carbon nanotubes compared to the catalyst supported on Vulcan. It demonstrates the influence of the support material for methanol oxidation.

4. Conclusions

A systematic study was carried out on the performance of Pt-Ru catalyst supported on carbon nanotube for methanol oxidation. The superiority of the carbon nanotube as catalyst support, compared to Vulcan, in the electrooxidation of methanol (and hence oxidation of CO) on Pt-Ru catalyst was demonstrated in the present study. Considering the results obtained from CO stripping studies, the necessity of proposing new methods for the evaluation of the electroactive area of nanostructured materials supported on nanostructured catalyst supports was established. Through electrochemical impedance analysis, it was possible to describe the various stages of methanol oxidation reaction, i.e., the de-hydrogenation and oxidation of CO_{ads}, by applying different potentials and/or varying the methanol concentration. This technique made it possible to control each and every one of these reaction steps and to demonstrate the predominance of each one. This permitted us to describe those conditions at which the bi-functional participation of Ru in methanol oxidation seems more important, demonstrating that CO oxidation takes place on Pt as well as on Ru.

Acknowledgements

The financial support for this project was given by CONACYT and DGAPA-UNAM through the projects CIAM 42146 and IN 109703, respectively. A.L.O. thanks CONACYT and IMP for a doctoral scholarship.

References

[1] A.S. Aricó, P. Cretí, P.L. Antonucci, J. Cho, H. Kim, V. Antonucci, Electrochim. Acta 43 (1998) 3719–3729.
[2] D. Chu, R. Jiang, Solid State Ionics 148 (2002) 591–599.
[3] R. Parsons, T. Vandernoot, J. Electroanal. Chem. 257 (1988) 9–45.
[4] K.L. Ley, R. Liu, C. Pu, Q. Fan, N. Leyarovska, C. Segre, E.S. Smotkin, J. Electrochem. Soc. 144 (1997) 1543–1548.
[5] C. Lamy, E.M. Belgsir, J.-M. Léger, J. Appl. Electrochem. 31 (2001) 799–809.
[6] W.H. Lizcano-Valbuena, V.A. Paganin, E.R. Gonzalez, Electrochim. Acta 47 (2002) 3715–3722.
[7] M. Watanabe, M. Uchida, S. Motoo, J. Electroanal. Chem. 229 (1987) 395–406.
[8] A. Hamnett, Catal. Today 38 (1997) 445–457.
[9] H.A. Gasteiger, N. Markovic, P.N. Ross, E.J. Cairnes, J. Phys. Chem. 98 (1994) 617–625.
[10] B. Gurau, R. Viswanathan, R. Liu, T.J. Lafrenz, K.L. Ley, E.S. Smotkin, E. Reddington, A. Sapienza, B.C. Chan, T.E. Mallouk, S. Sarangapani, J. Phys. Chem. B 102 (1998) 9997–10003.
[11] M. Watanabe, S. Motoo, J. Electroanal. Chem. 60 (1975) 267–273.
[12] T. Freelink, W. Vissher, A.P. Cox, J.A.R. van Veen, Electrochim. Acta 40 (1995) 1537–1543.
[13] K.A. Friedrich, K.P. Geyzers, U. Linke, U. Stimming, J. Stumper, J. Electroanal. Chem. 402 (1996) 123–128.
[14] S. Wasmus, A. Kuver, J. Electroanal. Chem. 461 (1999) 14–31.
[15] Y. Tong, H.S. Kim, P.K. Babu, P. Waszczuk, A. Wieckowski, E. Oldfield, J. Am. Chem. Soc. 124 (2002) 468–473.
[16] T. Freelink, W. Visscher, J.A.R. van Veen, Langmuir 12 (1996) 3702–3708.
[17] P. Waszczuk, A. Wieckowski, P. Zelenay, S. Gottesfeld, C. Coutanceau, J.-M. Leger, C. Lamy, J. Electroanal. Chem. 511 (2001) 55–64.
[18] D. Chu, S. Gilman, J. Electrochem. Soc. 143 (1996) 1685–1690.
[19] C. He, H.R. Kunz, J.M. Fenton, J. Electrochem. Soc. 144 (1997) 970–979.
[20] J.-H. Choi, K.-W. Park, B.-K. Kwon, Y.-E. Sung, J. Electrochem. Soc. 150 (2003) A973–A978.
[21] T. Schultz, S. Zhou, K. Sundmacher, Chem. Eng. Technol. 24 (2001) 1223–1233.

[22] A.J. Dickinson, L.P.L. Carrette, J.A. Collins, K.A. Friedrich, U. Stimming, Electrochim. Acta 47 (2002) 3733–3739.
[23] G.S. Chai, S.B. Yoon, J.-S. Yu, J.-H. Choi, Y.-E. Sung, J. Phys. Chem. B 108 (2004) 7074–7079.
[24] Z. He, J. Chen, D. Liu, H. Zhou, Y. Kuang, Diamond Relat. Mater. 13 (2004) 1764–1770.
[25] J. Guo, G. Sun, Q. Wang, G. Wang, Z. Zhou, S. Tang, L. Jiang, B. Zhou, Q. Xin, Carbon 44 (2006) 152–157.
[26] M. Carmo, V.A. Paganin, J.M. Rosolen, E.R. Gonzalez, J. Power Sources 142 (2005) 169–176.
[27] Y.-L. Yao, Y. Ding, L.-S. Ye, X.-H. Xia, Carbon 44 (2006) 61–66.
[28] J.T. Mueller, P.M. Urban, J. Power Sources 75 (1998) 139–143.
[29] J.T. Mueller, P.M. Urban, W.F. Holderich, J. Power Sources 84 (1999) 157–160.
[30] Y.-C. Liu, X.-P. Qiu, W.-T. Zhu, G.-S. Wu, J. Power Sources 84 (1999) 10–14.
[31] R.E. Melnick, G.T.R. Palmore, J. Phys. Chem. B 105 (2001) 9449–9457.
[32] R.E. Melnick, G.T.R. Palmore, J. Phys. Chem. B 105 (2001) 1012–1025.
[33] J. Otomo, X. Li, T. Kobayashi, C.-J. Wen, H. Nagamoto, H. Takahashi, J. Electroanal. Chem. 573 (2004) 99–109.
[34] I.-M. Hsing, X. Wang, Y.-J. Leng, J. Electrochem. Soc. 149 (2002) A615–A621.
[35] W. Sugimoto, K. Aoyama, T. Kawaguchi, Y. Murakami, Y. Takasu, J. Electroanal. Chem. 576 (2005) 215–221.
[36] A.S. Aricó, H. Kim, A.K. Shukla, M.K. Ravikumar, V. Antonucci, N. Giordano, Electrochim. Acta 39 (1994) 691–700.
[37] M. Jafarian, M.G. Mahjani, H. Heli, F. Gobal, H. Khajehsharifi, M.H. Hamedi, Electrochim. Acta 48 (2003) 3423–3429.
[38] J.C. Calabrese, L.F. Dahl, P. Chini, G. Longoni, S. Martinengo, J. Am. Chem. Soc. 96 (1974) 2614–2616.
[39] G. Longoni, P. Chini, J. Am. Chem. Soc. 98 (1976) 7225–7231.
[40] S.Lj. Gojkovic, T.R. Vidakovic, D.R. Durovic, Electrochim. Acta 48 (2003) 3607–3614.
[41] C. Bock, M.-A. Blakely, B. MacDougall, Electrochim. Acta 50 (2005) 2401–2414.
[42] J.W. Guo, T.S. Zhao, J. Prabhuram, R. Chen, C.W. Wong, Electrochim. Acta 51 (2005) 754–763.
[43] L. Jiang, G. Sun, X. Zhao, Z. Zhou, S. Yan, S. Tang, G. Wang, B. Zhou, Q. Xin, Electrochim. Acta 50 (2005) 2371–2376.
[44] T.J. Schmidt, M. Noeske, H.A. Gasteiger, R.H. Behm, P. Britz, H. Bonnemann, J. Electrochem. Soc. 145 (1998) 925–931.
[45] Z. Jusys, R.J. Behm, J. Phys. Chem. B 105 (2001) 10874–10883.
[46] P. Waszczuk, A. Wieckowski, P. Zelenay, S. Gottesfeld, C. Coutanceau, J.-M. Léger, C. Lamy, J. Electroanal. Chem. 511 (2001) 55–64.
[47] L. Dubau, F. Hahn, C. Coutanceau, J.-M. Léger, C. Lamy, J. Electroanal. Chem. 554–555 (2003) 407–415.
[48] M. Metikos-Hukovic, S. Omanovic, J. Mol. Catal. A: Chem. 136 (1998) 75–84.
[49] P. Liu, A. Logadottir, J.K. Norskov, Electrochim. Acta 48 (2003) 3731–3742.
[50] T. Iwasita, Electrochim. Acta 47 (2002) 3663–3674.
[51] J. Jiang, A. Kucernak, J. Electroanal. Chem. 543 (2003) 187–199.
[52] K. Kinoshita, P.N. Ross, J. Electroanal. Chem. 78 (1977) 313–318.
[53] W.H. Lizcano-Valbuena, V.A. Paganin, C.A.P. Leite, F. Galembeck, E.R. Gonzalez, Electrochim. Acta 48 (2003) 3869–3878.
[54] Y. Takasu, T. Kawaguchi, W. Sugimoto, Y. Murakami, Electrochim. Acta 48 (2003) 3861–3868.
[55] C.L. Green, A. Kucernak, J. Phys. Chem. B 106 (2002) 1036–1047.
[56] R. Cabrera-Sierra, M. Miranda-Hernández, E. Sosa, T. Oropeza, I. González, Corrosion Sci. 43 (2001) 2305–2324.
[57] T. Freelink, W. Visscher, J.A.R. van Veen, Surf. Sci. 335 (1995) 353–360.